CHEMICAL ENGINEERING TRANSACTIONS
VOL. 100, 2023
A publication of AIDIC
The Italian Association of Chemical Engineering
Online at www.cetjournal.it
Guest Editors: Sauro Pierucci, Flavio Manenti

ISBN 979-12-81206-03-8; **ISSN** 2283-9216
DOI: 10.3303/CET23100064

CFD Simulation and Verification of Distillation Sieve Tray Hydrodynamics by Clear Liquid Height

Javier A. Mancera-Apolinar[a,b,*], Diego F. Mendoza[c], Carlos A. M. Riascos[a]

[a]Universidad Nacional de Colombia; sede Bogotá. Departamento de Ingeniería Química y Ambiental-Grupo de Investigación de Bioprocesos; Carrera 30 # 45-03; Edificio 453. Bogotá-Colombia.
[b]Universidad de América. Departamento de Ingeniería Química y Ambiental; Avda Circunvalar No. 20-53. Bogotá-Colombia.
[c]Universidad de Antioquia. Departamento de Ingeniería Química. Calle 70 # 52-21, Medellín, Antioquia.
jamanceraa@unal.edu.co; javier.mancera@profesores.uamerica.edu.co

The present work consists of the simulation of a sieve tray using CFD for the air-water system, comparing the results obtained of the clear liquid height (h_{cl}), with the experimental data, adjusting and varying different characteristics. The investigation has two general steps: the first step was to modify the Grace Drag Model (GDM) based on experimental data of clear liquid height for different superficial gas velocities (V_s). Once this was achieved, in the second step were established the effects of different variables on the clear liquid height as: 1) type of geometry (2D and 3D), 2) height of the weir (h_w), 3) liquid load per weir length (Q_L/W) and 4) superficial gas velocity; in all the cases of the second step, the modified drag coefficient obtained in step 1 is used. Verification of predicted values for clear liquid height with experimental data demonstrated the accuracy of the proposed modeling in the modified drag coefficient. Results showed that the interphase momentum exchange (drag) coefficient can be estimated by the fitted GDM, concluding that Bennet correlation is not necessary to estimate gas hold-up as it is used in most research involving CFD to simulate sieve trays. The percentage of error in the proposed CFD model was around 3.42 % compared with the 40.0 % average reported in previous studies. These results generate new guidelines toward best practices for modeling the hydrodynamics in sieve trays.

1. Introduction

Distillation is a separation process of major importance in chemical and petroleum industries worldwide. It is also the most studied one due to its energy consumption. The prediction and the increase of separation efficiency have been major tasks in the design and operation of distillation columns. Efforts to maximize the efficiency of distillation columns are still justified on economic grounds and environmental impact due to its great energy consumption (Gorak & Sorensen, 2014).

Distillation column internals are directly related to the performance and efficiency; sieve trays are one of the most common internals in distillation equipment due to design simplicity, low cost, and reduced construction time. Due to the widespread use of this kind of trays, some attempts have been made to accurately simulate sieve tray hydrodynamics using Computational Fluid Dynamics (CFD), (Gesit et al., 2003; Krishna et al., 1999). However these CFD simulations showed that the interphase momentum exchange (drag) –estimated using Bennett correlation (Bennett et al., 1983) – fails to give accurate results compared with the experimental data for h_{cl}.

2. Mathematical model

When turbulence in bubbly flows is a concern, it is necessary to consider the continuous liquid phase based on the small density and small spatial scales of the dispersed gas. In this contribution is adopted a two-equation turbulence model based on the Reynolds Averaged Navier Stokes (RANS) approach for the liquid phase. The momentum exchange model considers drag, lift, virtual mass, and turbulent dispersion forces.

Paper Received: 16 February 2023; Revised: 15 April 2023; Accepted: 2 June 2023
Please cite this article as: Mancera-Apolinar J.A., Mendoza D.F., Riascos C.A., 2023, CFD Simulation and Verification of Distillation Sieve Tray Hydrodynamics by Clear Liquid Height, Chemical Engineering Transactions, 100, 379-384 DOI:10.3303/CET23100064

2.1 Flow equations

The main difficulty in a two-fluid model is the accurate representation of interphase forces and turbulence. The two-fluid model solves two sets of conservation equations for each phase; these equations include mass, momentum, and energy balances.

Continuity equation of liquid phase:

$$\frac{\partial(\alpha_L\rho_L)}{\partial t} + \nabla\cdot(\alpha_L\rho_L u_L) = 0 \quad (1)$$

Continuity equation of vapor phase:

$$\frac{\partial(\alpha_G\rho_G)}{\partial t} + \nabla\cdot(\alpha_G\rho_G u_G) = 0 \quad (2)$$

Where ρ_L, ρ_G, u_L and u_G are the liquid and gas phase densities and velocities, respectively.

The momentum equations for liquid and vapor phases correspond to:

$$\frac{\partial(\alpha_L\rho_L u_L)}{\partial t} + \nabla\cdot(\alpha_L\rho_L u_L u_L) = -\alpha_L\nabla P + \nabla\cdot[\alpha_L\mu_L^e(\nabla u_L + (\nabla u_L)^T)] + \alpha_L\rho_L g + F_{LG} \quad (3)$$

$$\frac{\partial(\alpha_G\rho_G u_G)}{\partial t} + \nabla\cdot(\alpha_G\rho_G u_G u_G) = -\alpha_G\nabla P + \nabla\cdot[\alpha_G\mu_G^e(\nabla u_G + (\nabla u_G)^T)] + \alpha_G\rho_G g + F_{GL} \quad (4)$$

Where P, μ_i^e and g correspond to pressure, effective viscosity ($\mu_L^e = \mu_{lam,L} + \mu_{t,L}$; $\mu_G^e = \mu_{lam,G} + \mu_{t,G}$), and gravity, respectively. The first term on the left side of each equation is the momentum accumulation in the phase, while the second one is the net momentum outlet from the phase.

The momentum exchange at the liquid-vapor interface, F_{LG} or F_{GL}, considers drag, lift, virtual mass, and turbulent dispersion forces:

$$F_{LG} = F_{LG}^{drag} + F_{LG}^{lift} + F_{LG}^{VM} + F_{LG}^{TD} = -F_{GL} \quad (5)$$

where

$$F_{LG}^{lift} = C_l\alpha_G\rho_L(u_G - u_L)(\nabla u_L) \quad (6) \qquad F_{LG}^{VM} = C_{VM}\alpha_G\rho_L\frac{D}{Dt}(u_G - u_L) \quad (7) \qquad F_{LG}^{TD} = -C_{TD}k\frac{\mu_{t,L}}{0.9\rho_L}\left(\frac{\nabla\alpha_G}{\alpha_G} - \frac{\nabla\alpha_L}{\alpha_L}\right) \quad (8)$$

According to Wang et al., (2006), C_l, C_{VM}, and C_{TD}, were set to be 0.5, 0.25, and 0.7, respectively.

2.2 Drag model

In multiphase flows, the correlations of interfacial forces describe and quantify the interaction between different phases. The interaction between liquid and gas phases is dominated by the drag force, and it is established by solving the momentum equations (Krishna & van Baten, 2003). The drag force is calculated as:

$$F_{LG}^{drag} = \frac{3C_D}{4d_b}\alpha_G\rho_L|u_G - u_L|(u_G - u_L) \quad (9)$$

where C_D is the drag coefficient, which can be obtained from the model developed by Grace et al., (1978). Grace's model is well suited for gas-liquid flows in which the bubbles exhibit a range of shapes, such as a sphere, ellipsoid, and spherical cap. The drag coefficient for different shapes of bubbles is calculated as:

$$C_D = \max\left(\min\left(C_{D,ellipse}, C_{D,cap}\right), C_{D,sphere}\right) \quad (10)$$

Where

$$C_{D,sphere} = \begin{cases} 24/Re_b & Re_b < 0.01 \\ 24\left(1 + 0.15Re_b^{0.687}\right)/Re_b & Re_b \geq 0.01 \end{cases} \quad (11) \qquad C_{D,cap} = \frac{8}{3} \quad (12) \qquad C_{D,ellipse} = \frac{4}{3}\frac{gd_b}{U_t^2}\frac{(\rho_L - \rho_G)}{\rho_G} \quad (13)$$

$$Re_b = \frac{\rho_l|\boldsymbol{u}_G - \boldsymbol{u}_L|d_b}{\mu_L} \quad (14) \qquad U_t = \frac{\mu_l}{\rho_L d_b}Mo^{-0.149}(J - 0.857) \quad (15)$$

where Mo, the Morton number, and J, a piecewise function, are calculated as:

$$Mo = \frac{\mu_L^4 g(\rho_L - \rho_G)}{\rho_L^2\sigma^3} \quad (16) \qquad J = \begin{cases} 0.94H^{0.757} & 2 < H < 59.3 \\ 3.42H^{0.441} & H > 59.3 \end{cases} \quad (17) \qquad H = \frac{4}{3}EoMo^{-0.149}\left(\frac{\mu_L}{\mu_{ref}}\right)^{-0.14} \quad (18)$$

where $\mu_{ref} = 0.0009\,kg/(m\,s)$ and Eo is the Eötvös number, defined as $Eo = \frac{g(\rho_L - \rho_G)d_b^2}{\sigma}$

2.3 Customized drag model

The Grace model for sieve-tray simulations is based on a balance of forces acting on a single bubble moving freely under gravity within a liquid (Grace et al., 1976). Since the present study aims to model bubble swarms, Grace's drag coefficient is modified as follows:

$$C_{D,correction} = F_{corr}C_D \quad (19)$$

where C_D is the drag coefficient calculated through the Grace model (Eq. 10) and F_{corr} is a correction factor. This factor was formulated as a function of superficial velocity of the fluid, following the work of Liang et al., (2016) and it was further adjusted with the aid of experimental data on clear liquid height and superficial gas velocity (Krishna et al., 1999).

3. Methodology

In the present investigation is simulate a sieve tray of the system air-water based on the work of Krishna et al., (1999). For the development of this study, two general steps were established:
1. Drag coefficient adjustment using CFD.
2. Analysis of the effect of different variables on h_{cl} by CFD.

Step 1
The first step consists of carrying out CFD simulations of the perforated plate, modifying the drag coefficient through the correction factor (Eq. 19), adjusting it to the experimental data of h_{cl} at three different surface velocities of the gas: 0.5, 0.7 and 0.9 m/s, a h_w of 80 mm and a Q_L/W of 8.25×10^{-4} $m^3/s.m$. It is proposed that the percentage deviation of the fit does not exceed 3 % compared to the experimental data. The least-squares method is used to find an equation for the correction factor as a function of the surface velocity of the gas. The boundary conditions for gas and liquid inlet are uniform profile and for gas and liquid outlet are pressure outlet; the condition for the wall is “no-slip wall”.

Step 2
In the second step, four cases are studied: in the first case, the effect of the variation of the type of geometry on the h_{cl} is studied, and it is compared with the experimental data of h_{cl} for h_w of 60, 80, 90 and 100 mm, to observe if there is a significant difference when working with a 2D geometry versus a 3D one. For Case 2, having selected the type of geometry given in Case 1, the results of h_{cl} varying the h_w are compared with the experimental data and with the Bennet correlation. In Case 3, Q_L/W is varied, the results of the h_{cl} are observed, and compared with the experimental data. In Case 4, the use of the function found in step 1 is verified concerning the experimental data of the h_{cl} and compared with the Krishna simulation and Bennett and Colwell correlations. Table 1 summarizes the methodology followed in this approach.

Table 1 Methodology for step 2.

Case	Fixed Variable	Variable evaluated	# simulations
1	V_S = 0.7 m/s; $Q_L/W = 8.25 \times 10^{-4}$ $m^3/s.m$; h_w: 60, 80, 90, 100 mm	Geometry: 2D and 3D	8
2	V_S = 0.7 m/s; $Q_L/W = 8.25 \times 10^{-4}$ $m^3/s.m$	h_w (mm): 60, 80, 90, 100	4
3	V_S = 0.7 m/s; h_w: 80 mm	Q_L/W (10^{-4} $m^3/s.m$): 4, 8.25, 12	3
4	$Q_L/W = 8.25 \times 10^{-4}$ $m^3/s.m$; h_w: 80 mm	V_S (m/s): 0.5, 0.7, 0.9	3

4. Simulations remarks

Simulations were done with ANSYS-Fluent® V18.0 on a Dell Intel Xeon W3530 2.8 GHz. Tray geometry was defined based on the work developed by Krishna et al., (1999). The Air-Water system was simulated within the two-phase Eulerian framework, with a standard k-ε model to compare it with the experimental data of h_{cl}. The solution scheme for Pressure-Velocity coupling was SIMPLE; and for spatial discretization and the transient formulation was first-order upwind. The geometry and mesh used in the simulations are shown in Figure 1. The mesh used was a hexahedral mesh to guarantee the maximum mesh quality and minimize convergence errors due to mesh configuration.

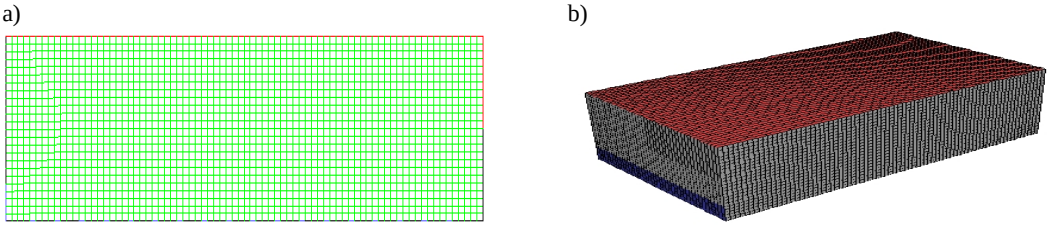

Figure 1. Mesh and flow geometry. a) 2D b) 3D system domains.

Detailed boundary conditions of the system in the CFD simulation are shown in Figure 2.
The initial conditions used in the tray simulations consist of a sieve tray full of air and an inlet linear velocity of gas and liquid obtained of the superficial gas velocity and liquid load respectively. The transport equations for additional scalars are assumed to have the form of the general scalar convective-diffusion equation. The convergence absolute criteria for the simulations were 1×10^{-3} for most variables except for the volume fraction which is 1×10^{-4}. For the time-dependent term, implicit first-order backward time differencing was used with a fixed time step of 1×10^{-3} seconds. The simulation was developed with smaller under-relaxation factor values than 0.8.

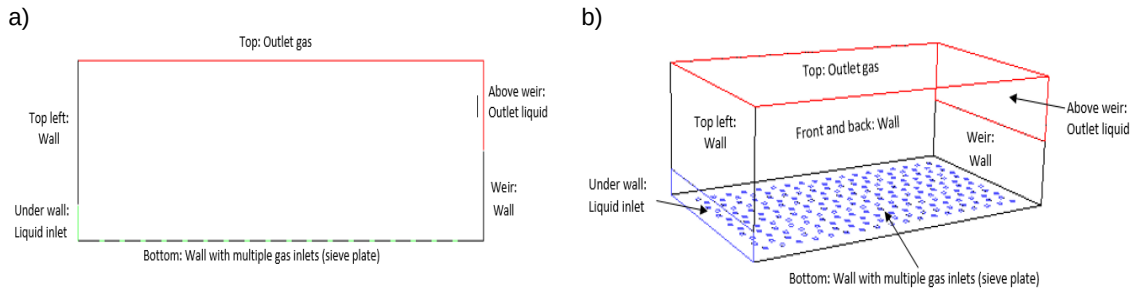

Figure 2. Inlets, outlets, and walls in geometries. a) 2D, b) 3D.

The 2D and 3D simulations took two and seven days to reach the steady state, respectively, this steady state is achieved until no more changes in the total liquid hold-up in the system are observed for a period large enough to obtain a time average.

5. Results and discussion

The results found of the F_{corr} for the three superficial velocities that fit the experimental data of the h_{cl} are presented in Table 2.

Table 2. Results F_{corr} of step 1 according to V_s

V_s (m/s)	F_{corr}	h_{cl} calculated with the F_{corr}	h_{cl} experimental	% deviation
0.5	0.07	0.042	0.0418	0.48 %
0.7	0.04	0.0398	0.0387	2.84 %
0.9	0.03	0.034	0.0343	0.87 %

The equation found by least squares for the calculation of the correction factor was:

$$F_{corr} = 0.25V_s^2 - 0.45V_s + 0.2325 \qquad 0.5 \leq V_s \leq 0.9 \tag{20}$$

The use of this equation is limited to the fulfillment of the following relation with the purpose that weeping is not present on the plate (Treybal, 1981):

$$\frac{V_s A_a}{N_h A_h} > \frac{0.0229\sigma}{\mu_G}\left(\frac{\mu_G^2}{\sigma\rho_G d_h}\frac{\rho_L}{\rho_G}\right)^{0.379}\left(\frac{l}{d_h}\right)^{0.293}\left(\frac{2A_a d_h}{\sqrt{3}p'^3}\right)^{2.8/\left(z/d_h\right)^{0.724}} \tag{21}$$

Case 1: Figure 3 shows the difference between 2D and 3D simulations. These results do not show significant differences between the 2D and 3D domains. Based on that, it was decided to work with the 2D system to reduce computational effort and, consequently, calculation time.

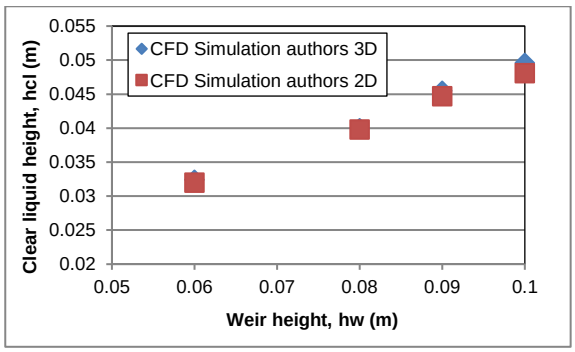

Figure 3. Comparison of clear liquid height in 3D and 2D simulation for approach 1. V_s = 0.7 m/s. QL/W = 8.25 x 10-4 m3/s m.

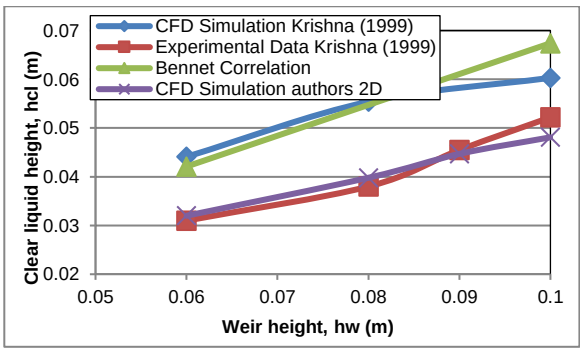

Figure 4. Clear liquid height vs weir height. V_s = 0.7 m/s; QL/W=8.2x10-4 m3/s m.

Additionally, 2D simulations are more stable from the numerical point of view because the calculation is reduced by one dimension. The small difference between 2D and 3D is mainly because the same and unique bubble size was used for both geometries. In addition to the above, the meshes of the two geometries have very similar elements, as well as their characteristics: 2D is rectangular and 3D is hexahedral. Furthermore, the setup is analogous with equivalent initial and boundary conditions.

Case 2: Figure 4 shows the results of 2D simulation performed in this case; it can be seen that they fit the experimental data better than the results obtained by Krishna's simulation and Bennet correlation. This

improvement is due to the adjustment made to the drag coefficient through the drag correction factor.The performance of Krishna's model is similar to Bennnet's because the first one uses an adjustment through Bennet correlation to initialize the simulations and bring the convergence to a specific value of gas hold up; while simulations developed in the present work are independent of Bennet correlation. It is important to mention that Krishna simulated six seconds, the time average it takes for the simulation to stabilize, while the simulations performed in this study took 40 seconds, possibly due to the adjustment of the coefficient, which increases the stabilization time of the simulation but with results closer to the experimental data.Table 3 presents the individual and averaged errors of results from Krishna's simulation, Bennet's correlation, and this research. These errors were calculated against the experimental data at the same operational conditions. This confirms the proposed model presents the lowest error.

Table 3. Percentage of error of the different simulations and correlation against the experimental data for V_S = 0.7 m/s; Q_L/W=8.2x10^{-4} m^3/m s.

Weir height (m)	Krishna	Bennet	This work
0.06	42.3 %	35.8 %	3.2 %
0.08	45.8 %	44.2 %	2.84 %
0.09	N/A	34.3 %	1.8 %
0.1	15.5 %	29.1 %	7.9 %
Average	**34.5 %**	**35.9 %**	**3.93 %**

Case 3: the Figure 5 shows the results of the h_{cl} for different Q_L/W, where the effectiveness of the adjustment of the drag coefficient is observed. In this figure, the similarity between Krishna's simulation and Bennet correlation can be appreciated again.

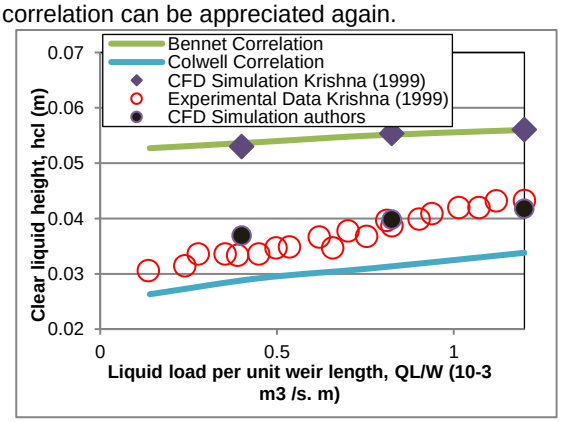

Figure 5. Clear liquid height vs liquid weir load. hw=80 mm; V_S= 0.7 m/s

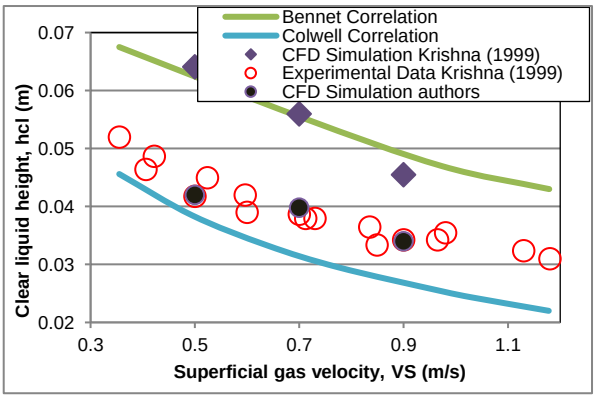

Figure 6. Clear liquid height vs superficial gas velocity. hw=80 mm, QL/W=8.2x10-4 m3/s m.

Table 4 presents the individual and averaged errors of results from Krishna's simulation, Bennet and Colwell correlations, and this work, against the experimental data for weir height 80 mm and superficial gas velocity 0.7 m/s. The better average error of our model is a consequence of the fact that initialization and convergence are not forced to meet the estimations by Bennet correlation, as in previous works.

Table 4. Percentage of error of the different simulations and correlations against the experimental data for h_w = 80 mm; V_S = 0.7 m/s.

Liquid weir load (10^{-3} m^3/m s)	Krishna	Bennet	Colwell	This work
0.4	55.88 %	58.82 %	14.71 %	8.53 %
0.825	39.55 %	38.54 %	21.91 %	2.84 %
1.2	29.56 %	29.33 %	21.48 %	3.46 %
Average	**41.66 %**	**42.23 %**	**19.37 %**	**4.94 %**

Case 4: Figure 6 shows that simulations performed, at the different superficial gas velocities proposed in the methodology, are more accurate than those performed by Krishna, and Bennett, and Colwell correlations, verifying the effectiveness of the adjustment of the drag coefficient implemented.Table 5 presents the individual and averaged errors of results from Krishna's simulation, Bennet and Colwell correlations, and this work, against the experimental data, for height weir 80mm and liquid load 8.2x10^{-4} m^3/(m.s). Once again, the proposed model performs more accurately due to its independence with Bennet correlation for the initialization and simulation. The average errors evidence a better performance of our model. Table 6 summarizes the error of the different simulations results for the proposed model and Krishna's results against the experimental data.

Table 5. Percentage of error of the different simulations and correlations against the experimental data for h_w= 80mm; $Q_L/W=8.2x10^{-4}$ m^3/m s.

Superficial gas velocity (m/s)	Krishna	Bennet	Colwell	This work
0.5	53.35 %	50.0 %	8.13 %	0.48 %
0.7	47.37 %	46.32 %	24.88 %	2.84 %
0.9	30.37 %	40.69 %	35.89 %	0.87 %
Average	**43.7 %**	**45.67 %**	**22.97 %**	**1.40 %**

Table 6. Average error for this work and Krishna's simulations.

Case	This work	Krishna
2	3.93 %	34.5 %
3	4.94 %	41.66 %
4	1.40 %	43.70 %
Average	**3.42 %**	**40.0 %**

6. Conclusions

The model developed in this work was accurately implemented; this was demonstrated through a quantitative validation using the error against experimental data. The percentage of general deviation of the results obtained by CFD of the hcl concerning the experimental data in the simulations was 3.42 %. The error values in the model of this work (3.2 %) outperforms Krishna's simulations (40 %). Furthermore, the validation implemented for the different models showed a better performance for our model than for the models proposed by Krishna, Bennet, and Cowell. The correction of the drag coefficient as function of superficial gas velocity is a good alternative to include the effect of multi bubbles interacting as a swarm. The obtained results lead to conclude that for this type of two-phase system with turbulence, a 2D domain approximation is a good way to optimize resources in terms of computational time. This simplification can be used without losing critical accuracy in the model.

Nomenclature

α – void fraction, --
σ – Surface tension, N/m
μ_{lam} – Laminar viscosity, kg/m.s
μ_t – turbulent viscosity, kg/m.s

Acknowledgments

The authors acknowledge the financial support of Universidad Nacional de Colombia and Colciencias under the 617 grant, and the collaboration and advice of Professor Ronnie Andersson.

References

Bennett, D. L., Agrawal, R., & Cook, P. J. (1983). New pressure drop correlation for sieve tray distillation columns. *AIChE Journal*, *29*(3), 434–442. https://doi.org/10.1002/aic.690290313

Gesit, G., Nandakumar, K., & Chuang, K. T. (2003). CFD modeling of flow patterns and hydraulics of commercial-scale sieve trays. *AIChE Journal*, *49*(4), 910–924. https://doi.org/10.1002/aic.690490410

Gorak, A., & Sorensen, E. (2014). *Distillation: Fundamentals and Principles*. Academic Press.

Grace, J. R., Wairegi, T., & Brophy, J. (1978). Break-up of drops and bubbles in stagnant media. *The Canadian Journal of Chemical Engineering*, *56*(1). https://doi.org/10.1002/cjce.5450560101

Grace, J. R., Wairegi, T., & Nguyen, T. H. (1976). Shapes and velocities of single drops and bubbles moving freely through immiscible liquids. In *Trans Inst Chem Eng* (Vol. 54, Issue 3).

Krishna, R., & van Baten, J. M. (2003). Modelling sieve tray hydraulics using computational fluid dynamics. *Chemical Engineering Research and Design*, *81*(1), 27–38. https://doi.org/10.1205/026387603321158168

Krishna, R., van Baten, J. M., Ellenberger, J., Higler, A. P., & Taylor, R. (1999). CFD simulations of sieve tray hydrodynamics. *Chemical Engineering Research and Design*, *77*(7), 639–646. https://doi.org/10.1205/026387699526575

Liang, X. F., Pan, H., Su, Y. H., & Luo, Z. H. (2016). CFD-PBM approach with modified drag model for the gas–liquid flow in a bubble column. *Chemical Engineering Research and Design*, *112*, 88–102. https://doi.org/10.1016/j.cherd.2016.06.014

Treybal, R. E. (1981). Mass Transfer Operations 3th edition. In *McGraw-Hill*.